Advanced Composites for Aerospace, Marine, and Land Applications II
Edited by: T. Sano and T.S. Srivatsan
TMS (The Minerals, Metals & Materials Society), 2015

INFLUENCE OF REINFORCEMENT CONTENT ON TENSILE RESPONSE AND FRACTURE BEHAVIOR OF AN ALUMINUM ALLOY METAL MATRIX COMPOSITE

K. Manigandan[1], T. S. Srivatsan[2], Zhencheng Ren[1] and Jingyi Zhao[1]

Division of Materials Science and Engineering
Department of Mechanical Engineering
The University of Akron
Akron, Ohio 44325-3903, **USA**
1: Graduate student; 2: Professor

Abstract

In this paper, the results of a study that examined the intrinsic influence of ceramic particulate reinforcements on tensile deformation and fracture behavior of aluminum alloy 2014 is presented and discussed. The candidate aluminum alloy was reinforced with two volume fractions of the alumina (Al_2O_3) particulates. Influence of particulate reinforcement on microstructural development is highlighted. Samples of the aluminum alloy-based metal matrix composite were deformed in uniaxial tension. The influence of nature of loading and intrinsic microstructural effects on stress versus strain response, mechanical properties, deformation and final fracture behavior are neatly elaborated and discussed in light of intrinsic microstructural effects, deformation characteristics of the microstructural constituents and nature of loading.

Keywords: aluminum alloy, ceramic particle reinforcement, metal-matrix composite, microstructure, tensile response, fracture behavior, mechanisms.

1. Introduction

Discontinuously-reinforced aluminum (DRA) alloy-based metal matrix composites (MMCs) containing particulate, whisker or short fiber reinforcements in a 2XXX, 6XXX or 7XXX series aluminum alloy metal matrix have in the time period spanning the last three decades, i.e., since the 1980's, engendered considerable scientific and technological interest for selection and use in automobile, aerospace and a spectrum of other high performance markets [1- 12]. These composites are preferred primarily because they offer a number of advantages. A few of these are a 15-40 pct. increase in strength and a 30-100 pct. increase in stiffness when compared with the unreinforced alloy [9, 13-15]. Besides, the metal-based composite maintains receptiveness to processing and characterization techniques that are traditionally used for the conventional unreinforced counterpart. Increase in modulus of greater than one hundred percent have been reported for aluminum alloy that is reinforced with a volume fraction of 40 pct. of silicon carbide [12]. From a design engineering perspective that attractiveness stems from an improvement in elastic modulus, i.e., density compensated increase in elastic modulus. The moduli obtained are greater than the values obtained for typical titanium alloys and only marginally less than those of steels. Besides, the DRA MMCs based on particulate reinforcements are attractive primarily because they can be made to have properties that are isotropic in three dimensions, or in a plane, when compared one-on-one with the continuously-reinforced metal matrices. Also, conventional secondary fabrication methods and metallurgical processing can be used to produce a wide range of product forms, making them relatively inexpensive when compared one-on-one with metal-based composites that are reinforced with continuous filaments. The discontinuously-reinforced metal matrices based on whisker reinforcements offer the potential for enhanced properties, but often tend to suffer from whisker damage and breakage during secondary fabrication [16, 17].

The use of discontinuous ceramic particle reinforcements in aluminum alloy metal matrices has been shown to provide attributes such as improved abrasion resistance [18], enhanced strength at high temperatures [19], improved creep rupture properties [20], good micro-creep performance [21], improved corrosion resistance [22], and enhanced resistance to fatigue crack initiation when compared one-on-one with the unreinforced matrix alloy [23]. The noticeable disadvantages with these materials are that they often suffer from low tensile ductility (quantified by elongation or strain to failure), inadequate fracture toughness and inferior fracture resistance compared to the unreinforced metal matrix [24-32]. In recent years the emerging DRA MMCs have been synthesized using the techniques of ingot metallurgy, powder metallurgy and mechanical alloying. Each of these techniques results in an MMC that has different microstructure and thus different properties.

The objective of this short technical manuscript is to present experimental evidence of the influence of particulate volume fraction on the tensile response of a ceramic particulate reinforced aluminum alloy based MMC. The tensile properties and resultant fracture behavior were evaluated for two different volume fractions of the discontinuous ceramic particle reinforcement phase in the aluminum alloy metal matrix. The material produced had the same matrix composition, aging condition, precipitation characteristics and reinforcement particle characteristics to include type, size distribution, shape and interfacial

characteristics. The quasi static fracture behavior of the two composites is discussed in light of concurrent and mutually interactive influences of intrinsic composite microstructural features, deformation characteristics of the metal matrix and the discontinuous particulate reinforcement phase.

2. Material

The DRA MMCs selected for this study were based on aluminum alloy 2014 reinforced with fine particulates of Al_2O_3. The ceramic particle–reinforced 2014 aluminum alloy MMCs were made using a proprietary casting technique by DURAL Aluminum Composites Corporation (DURALCAN USA, San Diego, CA). Two different fractions of the discontinuous Al_2O_3 particulate reinforcement phase (10 to volume percent and 15 volume percent) were chosen. The nominal chemical composition (in weight percent) of the matrix alloy is given in **Table 1**. The alloy has balanced levels of copper and magnesium, the primary strengthening agents. The iron and silicon elements in the alloy are impurities. The ingot-based Al_2O_3 particulate-reinforced MMC was made available as an extrusion billet. The billets were produced by extrusion of the cast ingot at 450°C through a standard shear-face die. The starting ingot was 178 mm in diameter and extruded at an extrusion ratio of 17:1 to produce rectangular blanks that measured 19 x 76 mm. The extruded 2014/Al_2O_3/ *xxp* (where *xx* denotes the volume percent of the discontinuous particulate reinforcement phase) material was solutionized at 500°C for 2 hours, cold water quenched, and artificially aged at 160°C for 2 hours to get the peak-elevated aged condition (T6). DURALCAN USA (California) provided the 2014/Al_2O_3/10*p* and 2014/Al_2O_3/15*p* MMCs, in the T6 condition.

Table 1: **Chemical Composition of matrix Al-Cu-Mg Alloy 2014 (in weight Percent)**

Element	Cu	Mg	Mn	Si	Al
Percent	4.4	0.50	0.80	0.80	Balance

3. Specimen Preparation

Blanks of size 150 x 20 x 20 mm were cut from the as-received 2014/Al_2O_3/10*p*-T6 and 2014/Al_2O_3/15*p*-T6 extrusions using a diamond-coated saw blade. Tension test specimens were precision machined from the blanks using a diamond-tipped cutting tool. The test specimens were machined with the stress axis parallel to the extrusion direction and conformed to specifications in ASTM E-8 [33]. The machined test specimens were smooth and cylindrical in the gage section, which measured 6.25 mm in diameter and 25 mm in length. To minimize the effects of any surface irregularities and finish, final surface preparation was achieved by mechanically polishing the entire gage section of the test specimens, prepared from the two MMCs, using progressively finer grades of silicon carbide–impregnated emery paper, to remove any and all circumferential scratches and surface machining marks.

4. Mechanical Testing

4.1 Initial Microstructure Characterization

Samples were cut from both the MMCs and prepared by standard metallographic procedures for observation in an optical microscope. The morphology of the reinforcing phase, i.e., the ceramic particulates (Al_2O_3), and their distribution through the aluminum alloy metal matrix and other observable intrinsic microstructural features were carefully examined in an optical microscope and photographed using a bright-field illumination technique.

4.2 Mechanical Testing

All mechanical tests were performed on a fully automated, closed-loop, servo hydraulic structural test machine (INSTRON: Model 8500 Plus) equipped with a 100 KN load cell. A precision alignment was given to the load train prior to the initiation of testing so as to eliminate and/or minimize grip-induced bending. Uniaxial tensile tests were carried out in the room temperature, laboratory air environment ($T = 23^oC$, Relative Humidity = 55 pct.). The specimens were deformed at a constant strain rate of 10^{-4}/s. An actual 12.5 mm gage-length clip-on extensometer was attached to the test specimen (made from the MMC material) at the gage section with rubber bands. The stress and strain variation, parallel to the load line, and resultant mechanical properties of stiffness, strength and ductility was provided as a computer output of the test machine.

4.3 Failure-Damage Analysis

Fracture surfaces of the deformed and failed tensile test specimens of the two chosen MMCs were comprehensively examined in a JEOL scanning electron microscope (SEM) to determine the following:

(i) Macroscopic fracture mode, and

(ii) To characterize the fine-scale topography and microscopic mechanisms governing final fracture.

The distinction between macroscopic and microscopic fracture mechanisms is based entirely on the magnification level at which the observations are made. Samples for observation in the SEM were obtained from the deformed and failed MMC specimens by sectioning parallel to the fracture surface.

5. Results and Discussion

5.1 Initial Microstructure

The optical micrographs illustrating the microstructure of the 2014/Al_2O_3/*xxp*-T6 composites are shown in **Figures 1 and 2**. The Al_2O_3 particulate reinforcement phases, in the 2014-aluminum alloy metal matrix, were (a) non-uniform in size, (b) irregularly shaped, and (c) dispersed randomly through the aluminum alloy metal matrix. Some of the reinforcing Al_2O_3 particulates had sharp corners. At regular intervals, a clustering or

agglomeration of the reinforcing Al_2O_3 particulates, of varying size and shape, was observed, resulting in local concentration of particulate-rich and particulate-depleted regions. An agglomerated site consisted of the smaller Al_2O_3 particulates, of varying sizes and shapes, intermingled selectively with a few larger Al_2O_3 particulates, which appeared either rectangular or oblong in shape. The degree of agglomeration or clustering of the reinforcing particulates was found to increase with an increase in the amount of the Al_2O_3 reinforcement phase in the 2014-aluminum alloy metal matrix. The non-uniform distribution of the reinforcing aluminum oxide (Al_2O_3) particulates along the three orthogonal directions (extrusion, long transverse, and short transverse) results in an anisotropic microstructure of the 2014/Al_2O_3/*xxp*-T6 composites. The alumina particles varied in size. However, no attempt was made, in this study, to determine the average particulate size and deviation for the two chosen MMC materials.

5.2 Tensile Properties

The tensile properties of the 2014/Al_2O_3/*xxp*-T6 MMCs, for two different volume fractions of ceramic particulate (Al_2O_3) reinforcement at ambient (27^oC) temperature are summarized in **Table 2**. The results are the mean values based on duplicate tests. Factors contributing to the improved stiffness and strength of the 2014/Al_2O_3/*xxp*-T6 composites can be found elsewhere [34, 36]. The ultimate tensile strength (σ_{UTS}) of the composite microstructure was only marginally greater than the tensile yield strength (σ_{YS}), providing sufficient evidence that the work hardening rate past yielding is low. In fact, the ultimate tensile strength followed the same trend as the yield strength of the composite. The improvement in strength of the 2014/Al_2O_3/15*p*-T6 composite over the 2014/Al_2O_3/10*p*-T6 counterpart was only marginal at ambient test temperature (27^oC). For both volume fractions of the particulate reinforcement phase in the aluminum alloy matrix, both the reduction in area and tensile ductility decreased with an increase in reinforcement content in the aluminum alloy metal matrix. The overall strain to failure (ε_f) of the 2014/Al_2O_3/*xxp* MMCs decreases with an increase in reinforcement content and is quite consistent with the observed decrease in both strength and stiffness with an increase in reinforcement content in the aluminum alloy metal matrix. Influence of Al_2O_3 particulate reinforcement content on engineering stress versus engineering strain response is shown in **Figure 3**. An increase in reinforcement content in the soft aluminum alloy metal matrix resulted in an observable decrease in ductility quantified by elongation or strain to failure.

Variation of true stress with true strain for the two composites is shown in **Figure 4**. This curve in the region of uniform plastic deformation follows the power law relationship

$$\sigma = K\,[\varepsilon_p]^n$$

Where n is the strain hardening exponent and K is the monotonic strength coefficient. An increase in reinforcement content in the soft aluminum alloy matrix does result in an increase in strain hardening exponent. For both composites the strain hardening values followed the trend shown by most metals and their alloy counterparts. The increase in strain hardening with increase reinforcement content was at best minimal.

Table 2: **A compilation of the room temperature tensile properties of 2014 Aluminum Alloy/Al_2O_3 Composites (T = 25°C).**

Material	Elastic Modulus		Yield Strength		UTS		Elongation GL=0.9" (%)	Reduction in Area (%)
	Ksi	GPa	ksi	MPa	ksi	MPa		
AA 2014/10P	12,444.0	85.8	81.20	560	82.70	570	4.20	**9.5**
AA 2014/ 15P	13,372.5	92.2	74.50	514	77.70	536	2.24	**6.6**

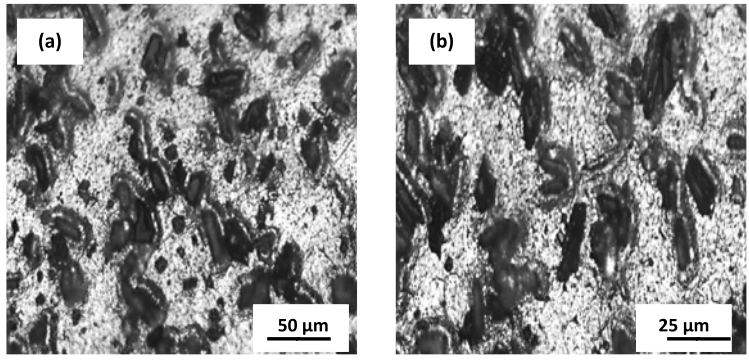

Figure 1. **Optical micrographs showing distribution of the reinforcing particulates in the 2014/Al_2O_3/10p composite**

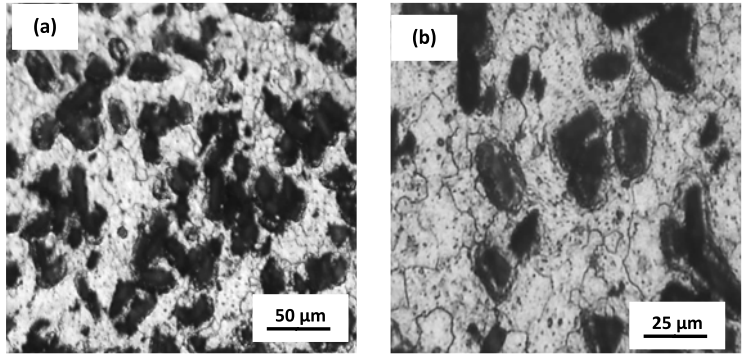

Figure 2. **Optical micrographs showing distribution of the reinforcing particulates in the 2014/Al_2O_3/15p composite.**

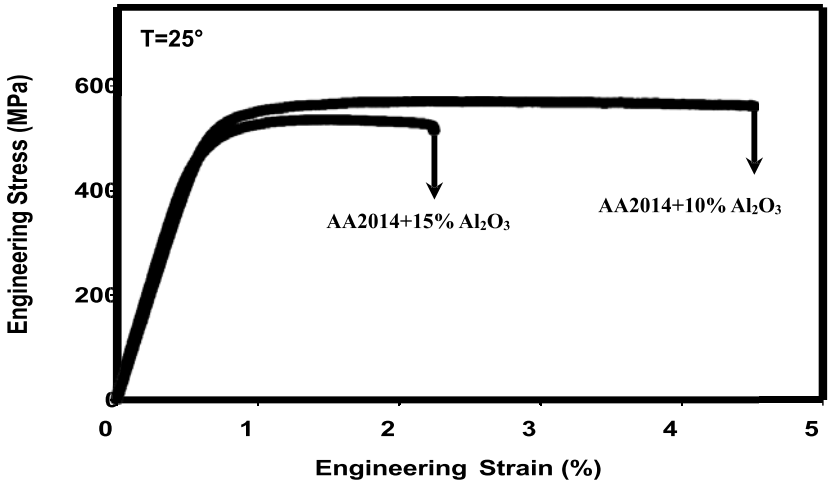

Figure 3. **Influence of particulate Al_2O_3 reinforcement on engineering stress versus engineering strain response of the two composites.**

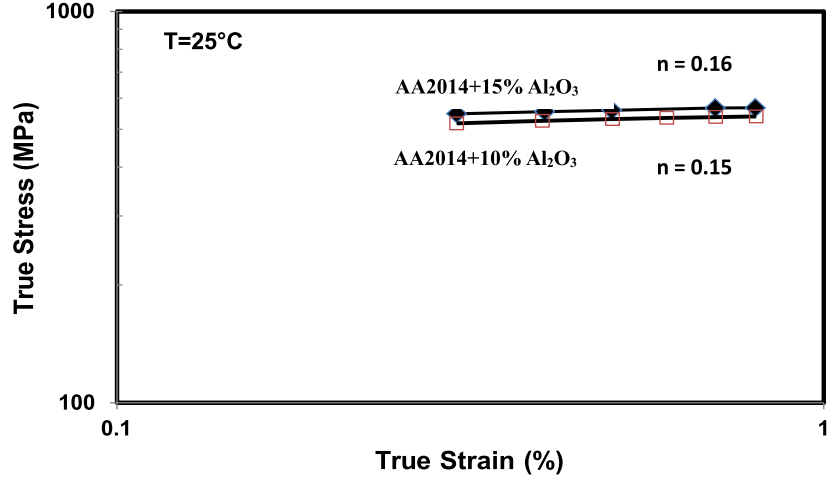

Figure 4. **The monotonic stress - strain response of the chosen composites. Increase in reinforcement content had a marginal influence on strengthening or hardening at the fine microscopic level.**

5.3 Tensile Fracture Behavior

The tensile fracture surfaces are helpful in providing information relevant to developing an understanding of intrinsic microstructural effects on fracture properties of the 2014/Al_2O_3/*xxp*-T6 composites. It is fairly well established by several researchers in their independent studies that the overall fracture behavior of unreinforced alloys is often dictated by events associated with void nucleation and growth, with nucleation essentially occurring at the coarse constituent particles dispersed through the microstructure [35, 36]. Furthermore, for the unreinforced aluminum alloy metal matrix, the nucleation of cavities and voids is promoted by the concurrent and mutually competitive influences of the following:

(1) Failure by cracking of the hard, brittle, and essentially elastically deforming second- phase inclusions and particles.

(2) Failure through separation at the interfaces between the elastically deforming Al_2O_3 particulate reinforcements and the plastically deforming aluminum alloy metal matrix.

At the ambient temperature (27^{o}C), the 2014/Al_2O_3/*xxp*-T6 composites exhibited limited ductility, on a macroscopic scale, with fracture occurring essentially normal to the tensile stress axis. High-magnification examination of the tensile fracture surfaces revealed features reminiscent of locally ductile and brittle mechanisms. Representative fractographs of the tensile fracture surface of the two composites, i.e., 2014/ Al_2O_3/10*p* and 2014/Al_2O_3/15p are shown in **Figures 5** through **Figure 8.**

Tensile fracture of the 2014/Al_2O_3/10*p* composite was relatively rough when viewed on a microscopic scale (Figure 5(a)). The reinforcing Al_2O_3 particulates were surrounded by ductile regions described as tear ridges (Figure 5(b)), particulate failure through cracking (Figure 5(c)), and failure through separation at the matrix-reinforcement interfaces (Figure 5(d)). Isolated pockets of voids were intermingled with tear ridges and isolated regions of dimpled rupture (Figure 6(c)). Failure of the particulate reinforcement was evident through both cracking (Figure 6a) and separation at the interfaces with the matrix (Figure 6(b)).

Tensile fracture of the 2014/Al2O3/15*p* composite was also flat and normal to the far-field stress axis when viewed on a macroscopic scale (Figure 7a), but rough when viewed on a microscopic scale (Figure 7(b)). The matrix of the composite revealed combinations of (a) tear ridges (Figure 7c)) and (b) failure of the reinforcing alumina particulates through cracking and separation at the interfaces with the matrix (Figure 7 (d)). The matrix of the composite was covered with isolated microscopic voids, of varying size and shape (Figure 8a). Multiple microscopic cracks were observed in regions of particulate agglomeration, which contributed to the observed degradation in tensile ductility (Figure 8b).

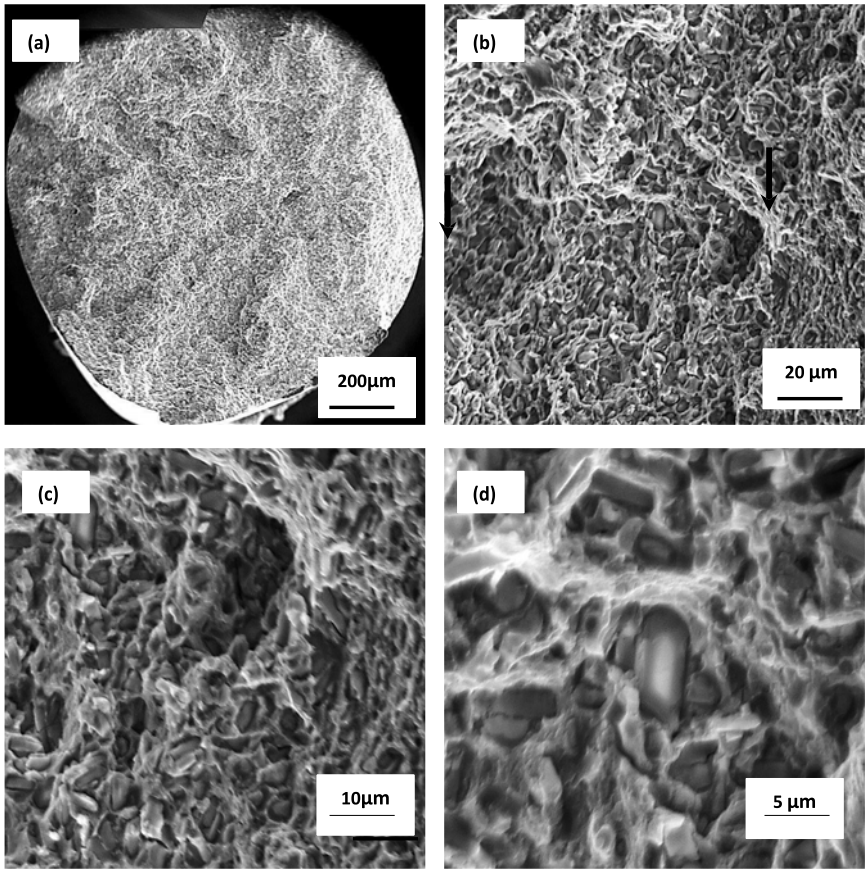

Figure 5. **Scanning electron micrograph of the tensile fracture surface of the 2014/Al_2O_3/10p composite deformed in tension showing:**

(a) Overall morphology of failure: rough on microscopic level

(b) Presence of tear ridges surrounding the reinforcing Al_2O_3 particulate reinforcements

(c) Failure of the reinforcing particulate through cracking

(d) Separation at the reinforcement – matrix interfaces

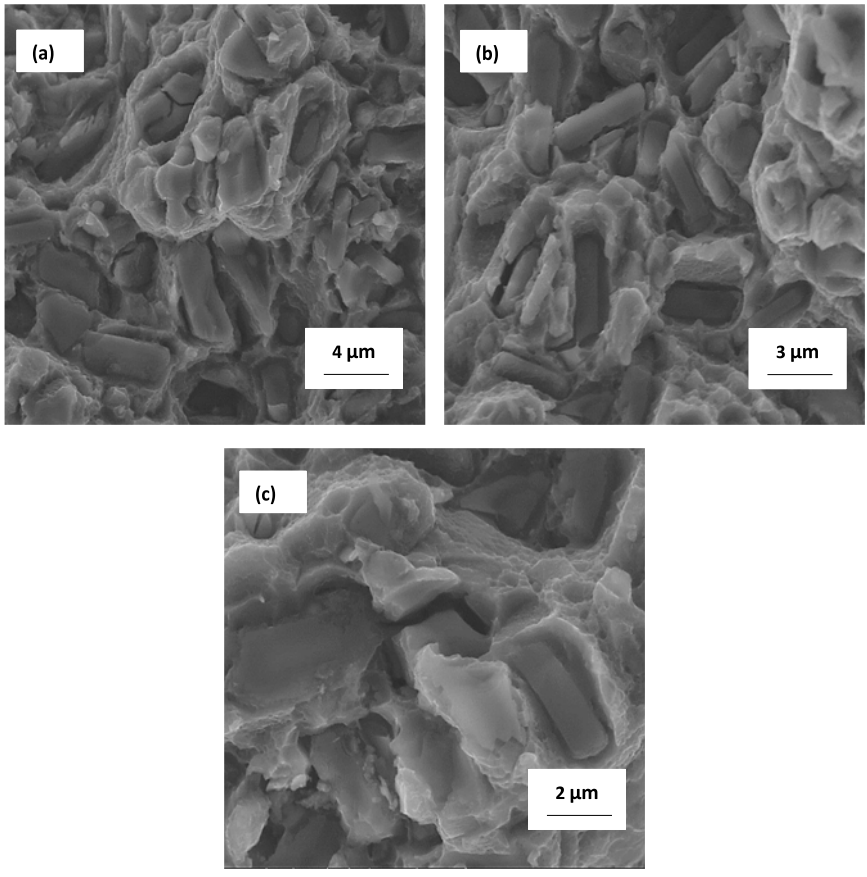

Figure 6. **Scanning electron micrograph of the tensile fracture surface of the 2014/Al_2O_3/10p composite deformed in tension showing:**
(a) Noticeable failure by cracking of the reinforcing particulates
(b) Clear and convincing evidence of separation at Al2O3 particulate -matrix interfaces.
(c) Isolated pockets of dimpled rupture

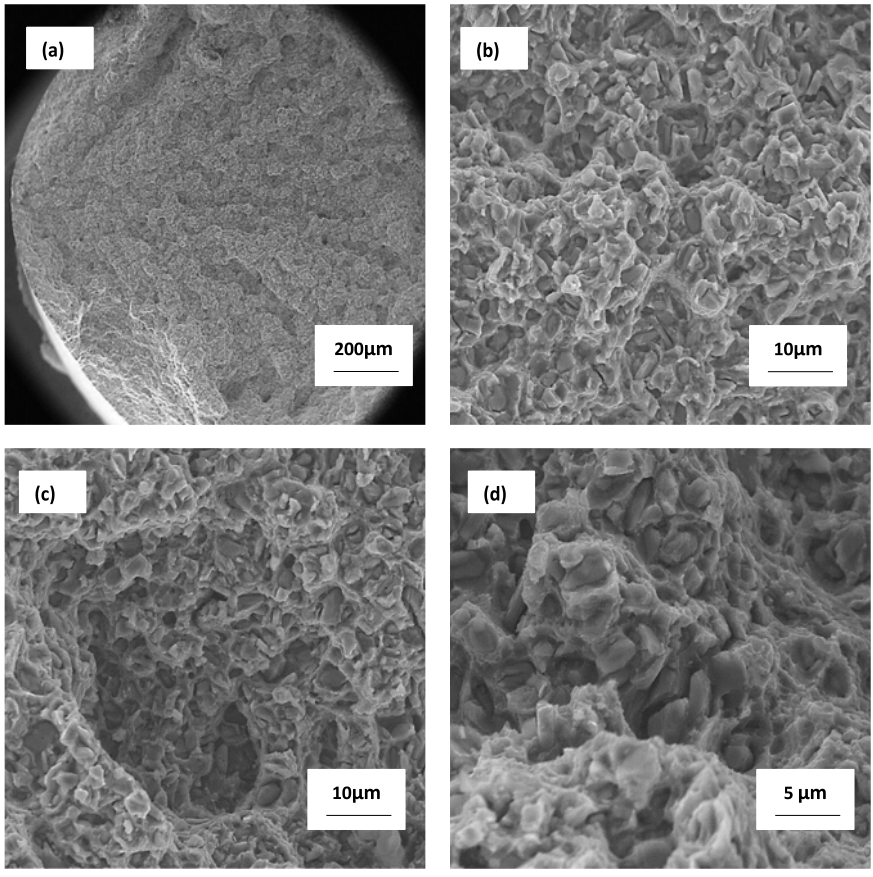

Figure 7. **Scanning electron micrograph of the tensile fracture surface of the 2014/Al_2O_3/15p composite deformed in tension showing:**

(a) Overall morphology of failure

(b) High magnification observation of (a) showing locally rough surface at fine microscopic level.

(c) High magnification observation of (b) showing tear ridges reminiscent of locally ductile failure

(d) Failure of the reinforcing Al_2O_3 particulates by both cracking and separation at the interfaces with the metal matrix.

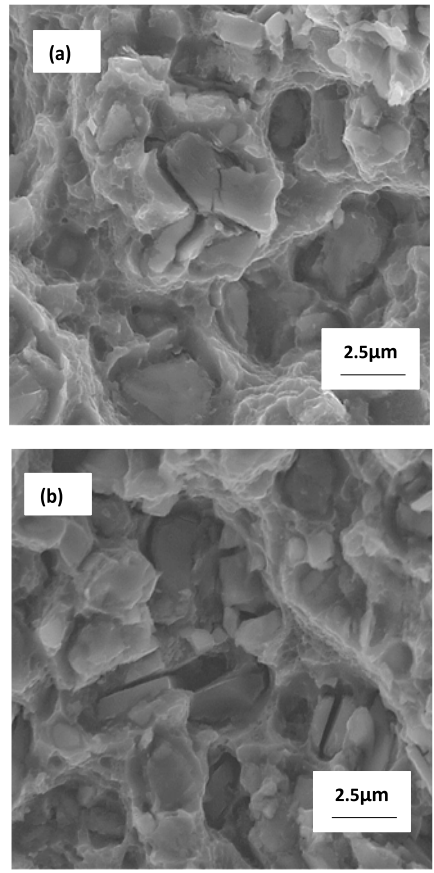

Figure 8. **Scanning electron micrograph of the tensile fracture surface of the 2014/Al_2O_3/15p composite deformed in tension showing:**
(a) Voids and shallow dimples scattered through the aluminum alloy metal matrix.
(b) Multiple microscopic cracks at regions of particulate agglomeration.

5.4 Microscopic Mechanisms Governing Fracture

The constraints in deformation caused by the presence of the hard, brittle, and essentially elastically deforming Al_2O_3 particles in the soft, ductile, and plastically deforming 2014 aluminum alloy metal matrix coupled with the resultant development of a triaxial stress state at the local level, in the metal matrix, aids in limiting the overall flow stress of the composite microstructure, while concurrently favoring the following events at the fine microscopic level:

(a) Void initiation and growth of voids in the matrix, and

(b) Failure by either cracking or separation at the reinforcement particulate-matrix interfaces.

Furthermore, as a consequence of the deformation constraints induced by the hard, brittle and elastically deforming Al_2O_3 particulate reinforcements, a higher applied stress is required to initiate plastic deformation in the adjoining matrix. This translates to higher elastic constant and higher yield strength of the composite material. Under the influence of a far-field tensile load, the microscopic voids appeared to have undergone limited growth confirming a possible contribution from particle constraint–induced triaxiality on failure of the composite matrix. Failure of the reinforcing Al_2O_3 particulate(s) is governed by competing influences of the following microscopic events: (1) local plastic constraints, (2) particle size, and (3) degree of agglomeration. The local plastic constraints are particularly important for the larger-sized particles and for particulate clusters during composite fracture [41].

A close examination of the fracture surfaces revealed the extent of damage to be highly localized at the Al_2O_3 reinforcing phase through cracked particles and failure at the interfaces of the reinforcing ceramic particle with the soft aluminum alloy metal matrix, with little evidence of void formation away from the cracked or fractured Al_2O_3 particle. This suggests that the plastic strain became localized during the early stages of deformation. The intrinsic brittleness of the reinforcing alumina particulates, coupled with the propensity for it to fracture due to localized deformation, results in both particle cracking and particle-matrix interface debonding (Figure 6 b and Figure 7 d) being the dominant damage mode. The higher yield strength, coupled with damage to the composite microstructure from the conjoint influence of cracking of the reinforcing Al_2O_3 particles and interfacial failure through decohesion, is responsible for the observed inferior ductility of the 2014/Al_2O_3/*xxp*-T6 MMCs. Also, the triaxial stresses generated during far-field tensile loading favor limited growth of the fine microscopic voids in the matrix of the composite. The limited growth of the voids during far-field tensile loading, coupled with lack of their coalescence as a dominant fracture mode for the two 2014/Al_2O_3/*xxp*- T6 MMCs studied, clearly indicates that the deformation properties of the 2014 matrix are significantly altered by the presence of the discontinuous Al_2O_3 particulate reinforcements. In Al_2O_3 particulate-rich regions of the matrix, fracture occurred early and the damage propagated rapidly among the reinforcing particle agglomerate. However, the reinforcement-lean regions, that is, the matrix, aid in retarding the progression and linkage of the damage.

Fracture of the brittle Al_2O_3 particles increases local damage and serve as a starting point for the formation of a long crack. This, in conjunction with failure of the surrounding

matrix, results in the formation of fine microscopic voids at the particle-matrix interfaces. Very few of the fine microscopic voids coalesce and the halves of these voids are the shallow dimples observed surrounding the cracked particles. The lack of formation of ductile dimples in the matrix, as a dominant fracture mode, can be attributed to the constraints imposed on plastic flow caused by the presence of discontinuous Al_2O_3 particles, that is, the deformation incompatibility between the plastically deforming metal matrix and the elastically deforming Al_2O_3 reinforcement phase, and not due to limited ductility of the 2014 aluminum alloy metal matrix. With an increase in reinforcement content, i.e., Al_2O_3, microscopic fracture was found to be dominated by cracking of the reinforcing particulates on account of their intrinsic brittleness. With a progressive increase in strain, the larger-sized particles fracture first, at low values of applied strain, followed by the smaller-sized particles.

The quasi-static fracture surfaces revealed the fracture plane of cracked particles to be essentially normal to the far-field stress, suggesting importance of normal (tensile) stress in inducing particle fracture. The overall "damage" resulting from quasi-static deformation of the $2014/A1_2O_3/xxp$ MMC can be associated with failure of the discontinuous particulate reinforcement either through cracking or separation at the interface of the particulate with the soft and ductile aluminum alloy metal matrix. An observation of the quasi-static fracture surfaces of the two composites revealed that an excess of 50 pct. of the reinforcing particles had fractured during deformation. This indicates that not all of the particles were loaded to their fracture stress, suggesting the non-uniform distribution of the particles in the metal matrix and their influence in governing deformation. This situation is exacerbated by the mismatch strain and concomitant high compression stresses in the composite matrix due to differences in the thermal expansion coefficient between the two key constituents of the composite: (i) the reinforcing Al_2O_3 particulates, and (ii) the 2014 aluminum alloy matrix [37, 38] For the reinforcing particles to fracture, the applied far-field tensile stress will have to first overcome the internal compressive stress present in the particle.

For this particulate-reinforced 2014 metal matrix, the majority of damage is associated with particulate clusters and is in the form of cracked particles and voids, which have formed around the particles. The broken Al2O3 particles elevate the local stress, which raises the probability of failure of the matrix and other particles in the immediate vicinity. Final fracture is achieved by damage propagation through the matrix between particle-rich regions. Few of the voids generated by particle cracking did not grow extensively in the tensile stress direction, which is generally the case in ductile fracture of unreinforced aluminum alloy [38]. The lack of extensive void growth in this Al_2O_3 particulate–reinforced 2014 aluminum alloy metal matrix suggests that the fracture strain is critically controlled by both the void nucleation strain and associated linkage strain.

6. Conclusions

The influence of volume fraction of discontinuous particulate reinforcement on tensile fracture of 2014 aluminum alloy–based MMCs provide the following key observations.

1. The as-received microstructure of the 2014/Al_2O_3-T6 composites revealed a non-uniform dispersion of the reinforcing particulates, of non-uniform size, along the different directions of the extruded composite plate. At regular intervals, an agglomeration or clustering of the Al_2O_3 particulates, of varying size, was observed.

2. The non-uniform size and dispersion of the reinforcing phase caused the particles to crack at low values of applied stress. The cracks initiated both at and near the particle- matrix interfaces and in regions of particle agglomeration.

3. The ultimate tensile strength (σ_{UTS}) of the composite microstructure was only marginally greater than the tensile yield strength (σ_{YS}), providing sufficient evidence that the work hardening rate past yielding is low. The ultimate tensile strength followed the same trend as the yield strength of the composite. The improvement in strength of the 2014/Al_2O_3/15*p*-T6 composite over the 2014/Al_2O_3/10*p*-T6 counterpart was only marginal at ambient test temperature (27^{o}C).

4. For both volume fractions of the particulate reinforcement phase in the aluminum alloy matrix, both the reduction in area and tensile ductility decreased with an increase in reinforcement content in the aluminum alloy metal matrix.

5. The quasi-static fracture surfaces revealed limited ductility or brittle appearance on a macroscopic scale but, at the microscopic level, features reminiscent of locally ductile and brittle rupture mechanisms. Tensile fracture of both the composites examined was relatively rough when viewed on a microscopic scale. The reinforcing Al_2O_3 particulates were surrounded by ductile regions described as tear ridges, particulate failure through cracking, and failure through separation at the matrix-reinforcement interfaces. Isolated pockets of voids were intermingled with tear ridges and isolated regions of dimpled rupture. Failure of the reinforcing Al_2O_3 particulates was evident through both cracking and separation at the interfaces with the soft metal matrix.

References

1. D. F. Hasson and C. R. Crowe: in 'Strength of Metals and Alloys, ICSMA 7' Pergamon Press, Oxford, 1985, pp.1515-1520
2. S. G. Fishman: 'Role of Interfaces on Material Damping' ASM, Materials Park, OH, 1985, pp. 33-41.
3. P. K. Liaw, H. G. Greggi, and W. A. Logsdon: ***Materials Science Letters***, 1987, 22, 1613
4. J. F. Mandell, K.C. Hong, and D. H. Grande: ***Ceramic Engineering Science***, Proc. 1987, 8, 937
5. D. H. Grande, J. F. Mandell, and K. C. J. Hong, ***Materials Science***, 1988, 23, 311
6. P. Niskanen, and W. R. Mohn:. ***Advances in Materials Processing***, 1988, 133, 39
7. M. S. Zedalis, J. D. Bryant, P. S. Gilman, and S. K. Das: ***Journal of Metals***, 1991, p. 29
8. Nair, S.V., Tien, J.K. and Bates, R.C**.** ***International Meals. Reviews***. 1985, 30, 285
9. T. S. Srivatsan, T. S. *Sudarshan and E. J. Lavernia:* ***Progress in Materials Science, An International Review Journal,*** Vol. 39 (4/5), 1995, pp. 317-325.
10. S. G. Fishman: Metal Matrix Composite Requirement: More Reliable Mechanical Properties Data, MMCIAC, Current Highlights, Vol. 1, May 1981.
11. W.C. Harrigan in Metal Matrix Composites (editors: R.JK. Everett and R. J. Arsenault) Academic Press, London, pp. 1-15, 1991.
12. R. J. Arsenault: ***Materials Science and Engineering***, Vol. 64, 1984, pp. 171-181.
13. W. R. East: ***Materials Engineering***, March 1988, p. 33.
14 R. DeMeis: ***Aerospace America***, March 1989, p. 26
15 T. C. Willis: ***Metals and Materials***, August 1988, p. 485
16 W. H. Hunt, Jr., C. R. Cook, and R. R. Sawtell: "Cost Effective High Performance Powder Metallurgy Aluminum Matrix Composites for Automotive Applications,' SAE Technical Paper Series 910834, February 1991, Warrendale, PA
17 W. H. Hunt, Jr., Paper presented at the International Conference on PM Aerospace Materials, November 1991, Lausanne, Switzerland
18. S. Norose, T. Sasdafa, and M. Okabe: in 'Proceedings 28th Japan Congress on Materials Research', 1985, pp. 231-241.
19 W.L. Phillips: in Proceedings of Conf. on Composite Materials' (Editor: B. Noton), Metallurgical Society of AIME, New York, 1978, pp. 567-577
20. T. G. Nieh: ***Metallurgical Transactions***, 1984, 15A, p. 139
21. G. Gould: in 'Proc. Third Int. Conf. on Isostatic Pressing', London, 1986, vol. 1, p. 10.
22. D. F. Hasson, C. R. Crowe, J. S. Ahearn, and D. S. Cooke: 'Failure Mechanisms in High Performance Materials', Cambridge University Press, Cambridge, 1985, pp. 147- 156
23. Y. Sugimura, and S. Suresh: ***Metallurgical Transactions***, 1992, 23A, p. 2231
24. P.K. Liaw abd W.A. Logsdon: ***Engineering Fracture Mechanics***, Vol. 24, 1986, pp. 737-745.
25. J. K. Shang and R. O. Ritchie: ***Metallurgical Transactions***, Vol. 20A, 1989, pp. 897- 908.
26. J. K. Shang and R. O. Ritchie: ***Acta Metallurgica***, 1989, Vol. 37, pp. 2267-2278.

27. J. J. Lewandowski, C. Liu and W. H. Hunt, Jr.: in Interfacial Phenomenon in Composites: Processing, Characterization and Mechanical Properties, TMS, AIME, Warrendale, PA, 1988.
28. J. J. Lewamdowski, C. Liu and W. H. Hunt, Jr.: ***Materials Science and Engineering***, Vol. 107A, 1989, pp. 49-55.
29. J. J. Lewandowski, C. Liu and W. H. hunt, Jr.: in Powder Metallurgy Composites (editors: P. Kumar, K. Vedula and A.M. Ritter), TMS-AIME, Warrendale, PA, 1989.
30. M. Manoharan and J. J. Lewandowski: ***Scripta Metallurgica***, Vol. 23, 1989, pp. 301- 305.

31. M. Manoharan and J. J. Lewandowski: ***Acta Metallurgica***, Vol. 38 (3), 1990, pp. 489- 496.
32. D. L. Davidson: ***Engineering Fracture Mechanics***, Vol. 33, 1989, pp. 965-977.
33. T.S. Srivatsan: ***Journal of Materials Science***, 1996, vol. 31, pp. 1375-88.
34. T.S. Srivatsan: "The Cyclic Fatigue and Fracture Behavior of Al2O3 Particulate- Reinforced 2014 Aluminum Alloy Metal-Matrix Compos2267-
35. F.A. McClintock: Ductility, ASM International, Metals Park, Cleveland, OH, 1968, pp. 256-61.
36. R.H. Van Stone, T.B. Cox, J.R. Low, Jr., and J.A. Psioda: ***International Metals Reviews***, 1975, vol. 30, pp. 157-71.
37. R.J. Arsenault, L. Wang, and C.R. Feng: ***Acta Metallurgica Materialia***., 1991.
38. A.S. Argon, J. Im, and R. Safoglu: ***Metallurgical Transactions*** A, 1975, Vol. 6A, pp. 825-837.
39. T.S. Srivatsan: ***International Journal of Fatigue***, 1995, vol. 17 (3), pp. 183-99.
40. D.J. Lloyd: Acta Metallurgica, 1991, vol. 39 (1), pp. 59-70.

41. E. Hochreiter, M. Panzenbock, and F. Jeglitsch: ***International Journal of Fatigue***, 1993, vol. 15 (6), p. 493.